Synthesis, Application, and Efficiency of the Cellulose@Fe3O4@ZIF-8 Carbon Aerogel Magnetic in the Removal of Gasoil from Aqueous Solutions

Elaheh Tajari
University of Kashan
Hadis Bashiri
hbashiri@kashanu.ac.ir

University of Kashan

Research Article

Keywords: Gasoil, Prosopis farcta, Metal-organic framework, Design of experiment, Adsorption, Cellulosic fibrous, Cellulose@Fe3O4@ZIF-8 carbon aerogel magnetic

Posted Date: March 26th, 2024

DOI: https://doi.org/10.21203/rs.3.rs-3939352/v1

Synthesis, Application, and Efficiency of the Cellulose@Fe_3O_4@ZIF-8 Carbon Aerogel Magnetic in the Removal of Gasoil from Aqueous Solutions

Elaheh Tajari and Hadis Bashiri*

Department of Physical Chemistry, Faculty of Chemistry, University of Kashan, Kashan, Iran

*Corresponding author: Tel: +98-31-5591-2336. E-mail: hbashiri@kashanu.ac.ir (H.Bashiri)

Abstract

Water pollution by Gasoil seriously threatens the environment and human health. Removing Gasoil from the aqueous solutions is critical to maintaining the safety and quality of the water source. This research looked at the feasibility of filtering Gasoil out of water. As a first step, we developed a new adsorbent from Prosopis farcta cellulose fibers by preparing a metal-organic magnetic framework (cellulose@Fe_3O_4@ZIF-8 carbon aerogel magnetic). The design of experiment method was utilized to explore how variations in pH, Gasoil concentration, and adsorbent dose influenced the elimination of Gasoil. Adsorbent has an adsorption capacity of 7 $g.g^{-1}$ and can adsorb 100 % of the petroleum floating in water. Time studies demonstrated no time dependence in the Gasoil adsorption process by the adsorbent. Freundlich isotherm described the adsorption of petroleum onto the prepared magnetic carbon aerogel. The free energy, enthalpy, and entropy changes as a part of the Gibbs thermodynamic equation were determined. The proposed magnetic carbon aerogel was an effective adsorbent for extracting petroleum from the aqueous solutions because of its rapid separation and high stability. Even after eight times of use, this adsorbent maintained its relatively high adsorption capacity, and only a 10% drop in adsorption efficiency was observed.

Keywords: Gasoil; Prosopis farcta; Metal-organic framework; Design of experiment; Adsorption; Cellulosic fibrous; Cellulose@Fe_3O_4@ZIF-8 carbon aerogel magnetic.

1. Introduction

The presence of Gasoil in water sources is particularly detrimental to plant/animal life and human health. Removing Gasoil from aqueous solutions is vital for protecting the safety and purity of water supplies. Various traditional techniques have been employed for polution removal, such as adsorption (Bashiri et al. 2020, Falaki &Bashiri 2021, Sarabadan et al. 2019), photocatalysts (Arabameri &Bashiri 2022, Jafarinejad et al. 2023, Simon et al. 2020), sedimentation (Chen et al. 2018, Sun et al. 2022), and ion exchange . However, these methods often suffer from restrictions such as low performance, cheapness, and complicated operation. Due to their promising adsorption capabilities and prospective uses in environmental remediation, metal-organic frameworks (MOFs) have engrossed much consideration in recent years as a unique class of porous materials. In this context, the extension of a highly efficient, profitable, and environmentally benign adsorbent based on MOFs is necessary for Gasoil removal from aqueous solutions (Karimi et al. 2021, Paz et al. 2023, Wu et al. 2019). MOFs are a porous material with a definite crystalline structure, a large surface area, and a pore size that can be modified by altering the concentration of metal ions or organic ligands. They have interesting characteristics that make them good candidates for many uses, such as gas storage, catalysis, and environmental remediation. The excellent thermal and chemical stability of Zeolitic Imidazolate Frameworks (ZIFs) has made them a prominent subclass within the larger family of MOFs (Kuwer et al. 2021).

ZIF-8, made up of Zinc ions coupled by imidazole ligands, is a water-stable MOF with an explicit microporous structure (Li et al. 2019). Heavy metal ion removal and dye removal from aqueous solutions are only two of the many uses that have prompted substantial research into the material (Zheng et al. 2014). The high surface area, broad pH stability, and feasible chemical interactions of ZIF-8 make it an ideal material for the adsorption of Gasoil and other contaminants (Bui et al. 2022b). Cellulosic fibrous materials derived from biomass have also shown potential as adsorbents for Gasoil removal. One such biomass is Prosopis farcta (PF), a renewable resource with abundant cellulose, hemicellulose, and lignin content (Liu et al. 2022). The magnetic properties of the composite material facilitate its easy separation and recovery from the aqueous solution, making it an ideal candidate for practical applications in water treatment (Gorkunov et al. 2002, Oliveira et al. 2002, Zeng et al. 2022).

Recent studies have shown that CelloMOFs have multifaceted applications such as water treatment, antibacterial, gas separation, and high-performance flexible supercapacitors (Abdelhamid &Mathew 2022, Jabbar et al. 2022, Liu et al. 2021, Tao et al. 2023, Tu et al. 2022, Zhou et al. 2019). These MOFs are a type of MOF that incorporate magnetic nanoparticles into their structure, resulting in materials with unique properties and applications (Nadar &Rathod 2018, Yadav et al. 2021, Zhao et al. 2015b). Magnetic MOFs can be utilized as sorbents to eliminate organic compounds from water. This category of MOFs has possible utilizations in various areas, including water treatment, catalysis, and biotechnology (Zhao et al. 2015a).

Research (Tajari &Bashiri 2023) looked at how well a magnetic MOF adsorbent constructed from the cellulose fibers of the PF plant worked in extracting Gasoil from aqueous. Preparation of the adsorbent includes design of experiment to determine the influence of factors on Gasoil treatment, including pH, Gasoil concentration, and adsorbent dose. This adsorbent had 7.5 $g.g^{-1}$ adsorption capacity, 100 times greater than iron-based adsorbents. Thus, the magnetic aerogel can efficiently extract gasoline from water. For removing Fosfomycin from pharmaceutical wastewater, a core-shell Fe_3O_4/PVP/ZIF-8 nanostructure adsorbent was generated (Abdelmigeed et al. 2022). The research evaluated the regeneration performance of the core-shell nanostructure adsorbent for Fosfomycin removal.

The adsorption efficacy of sonochemically produced Fe_3O_4@ZIF-8 for the elimination of copper ions from water is shown in another work (Bui et al. 2022a). It has a high maximal adsorption capacity (345 $mg.g^{-1}$), rapid adsorption time (10 min), and efficient elimination (95.3%). Heydari Moghadam et al. investigated zeolite imidazolate framework-8 (ZIF-8) to remove trichloroethylene from aqueous solutions with an optimum elimination efficiency of 96.29%. The adsorption capacity was 136.33 $mg.g^{-1}$. Trichloroethylene was demonstrated to be successfully removed from water by the ZIF-8 platform (Moghaddam et al. 2019). Khalilifard et al. used oleic acid- and graphene oxide-doped magnetic superhydrophobic polyurethane to separate organic species from aqueous solution. The magnetic sponges can be regulated and recycled using a magnet 15 times for oil spill cleaning without losing their adsorption ability. The modified sponge is an efficient adsorbent for treating oil in polluted water (khalilifard &Javadian 2021).

This research presents a novel adsorbent, cellulose@Fe_3O_4@ZIF-8 carbon aerogel magnetic, for Gasoil removal from aqueous solutions. It combines the advantages of biomass, magnetic Fe_3O_4 nanoparticles, and ZIF-8, resulting in a highly efficient, cost-effective, and environmentally friendly adsorbent material. The composite structure effectively overcomes the inherent limitations of ZIF-8, such as particle aggregation, and enables rapid Gasoil diffusion and adsorption. Design of Experiment (DOE) method, precisely the Box-Behnken method, is employed to optimize adsorption. Additionally, we investigate the adsorption isotherms, thermodynamics, and adsorption mechanism of the cellulose@Fe_3O_4@ZIF-8 carbon aerogel magnetic.

2. Experimental section

2.1. Materials and methods

Fe (III) chloride hexahydrate ($FeCl_3.6H_2O$, 99.0%), ethanol (96%), sodium citrate, sodium acetate, ethylene glycol, mercaptoacetic acid (MAA), zinc nitrate, methanol and 2-

methylimidazole have been purchased from Merck Company. Fruits of PF were collected from meadows in central Iran.

2.2. Synthesis of cellulose@Fe_3O_4@ZIF-8 carbon aerogel magnetic adsorbent

2.2.1. Preparation of Cellulosic Fibrous Biomass

PF is a renewable biomass resource, which was used as the cellulose fiber material. A mechanical grinder was used to reduce the size of the material to a finer consistency. They were then given several methanol washes.

2.2.2. Synthesis of Fe_3O_4 Nanoparticles

Fe_3O_4 Particles were successfully generated via a solvothermal approach. Using magnetic stirring for 30 minutes, 80 ml of ethylene glycol dissolved 2.7 g $FeCl_3.6H_2O$, 1.0 g sodium citrate, and 4.8 g NaAc. This mixture was sealed in a Teflon-lined stainless steel container and autoclaved at 473 K for 10 hours. Consequently, microspheres of Fe_3O_4 were collected, washed many times in ethanol, and then vacuum dried at 50 ℃. To make mercaptoacetic acid (MAA)-functionalized Fe_3O_4 nanoparticles, the following steps were taken: After shaking a mercaptoacetic acid (2.9 mM) ethanolic solution of 100 ml for 24 hours, 0.5 g Fe_3O_4 was added. The MAA-Fe_3O_4 nanoparticles were collected and washed.

2.2.3. Synthesis of cellulose@Fe_3O_4@ZIF-8 carbon aerogel magnetic

First, 6.4 g of $Zn(NO_3)_2$ and 14 g of prepared biomass were added to 20 ml of methanol. Then 1.0 g of MAA-Fe_3O_4 and 9.24 g of 2-methylimidazole are added and stirred for 2 hours at room temperature. After that, dry in a vacuum at 50 °C. Carbon aerogels were made by pyrolyzing cellulose@Fe_3O_4@ZIF-8 at 600°C for 1 hour in an N_2 environment in a tubular furnace. Then, magnetic cellulose@Fe_3O_4@ZIF-8 carbon aerogels were prepared.

2.3. Characterization of cellulose@Fe_3O_4@ZIF-8 carbon aerogel magnetic adsorbent

The cellulose@Fe_3O_4@ZIF-8 carbon aerogel magnetic adsorbent is identified using various analytical methods, including:

- Fourier Transform Infrared (FTIR) Spectroscopy: To examine the functional adsorbent groups in the sample and confirm the successful incorporation of ZIF-8 and Fe_3O_4 nanoparticles.
- X-ray Diffraction (XRD): To verify the ZIF-8 and Fe_3O_4 nanoparticle crystalline structure and to evaluate the composite material's stability.
- Scanning Electron Microscopy (SEM): To observe the morphology, size, and distribution of the ZIF-8 and Fe_3O_4 nanoparticles within the cellulosic fibers.
- Vibrating Sample Magnetometry (VSM): To assess the magnetic properties of the Fe_3O_4 nanoparticles within the composite material.
- Inductively Coupled Plasma emission spectroscopy (ICP): Analyze the amount of ions lost during the adsorption process due to ion leaching.

2.4. Adsorption experiments

First, a measured amount of Gasoil was dropped into the well of the culture dish's water. Afterward, a certain weight of adsorbent was carefully sprinkled over the top of the water-Gasoil solution. After Gasoil was adsorbed from water, the adsorbent was magnetically extracted and weighed. Adsorption of Gasoil onto an adsorbent occured within 10 seconds, which makes it a fast process. Equilibrium adsorption amount (q_e) and Gasoil removal ($R\%$) were determined using the following formulas:

$$q_e = \frac{m_2 - m_1}{m_1} \qquad (1)$$

$$R\% = \frac{m_2 - m_1}{m_g} \times 100 \qquad (2)$$

An initial mass of Magnetic - cellulose@Fe_3O_4@ZIF-8 carbon aerogel is m_1, a final mass of it is m_2, and m_g is used for initial mass of Gasoil (Shi et al. 2020, Tajari &Bashiri 2023).

2.5. Design of Experiment: Box-Behnken Method

The Box-Behnken DOE approach studied the effects of variables on the Gasoil removal by cellulose@Fe_3O_4@ZIF-8 carbon aerogel magnetic in an aqueous solution. This method helps determine the optimal parameters for the adsorption process, such as the mass of adsorbent (A), the mass of Gasoil (B), and the pH value (C). By systematically varying these parameters, it is possible to identify the conditions that result in maximum Gasoil removal efficiency. After that, we followed the blueprint and coded the independent variables' levels (-1, 0, 1 for low, medium, and high values) (Table 1). Table 2 shows the Box-Behnken design values for each independent variable and Design-Expert 13.0.5.0 trial outcomes.

Table 1. Experimental range and level of independent variables for Gasoil removal by the cellulose@Fe_3O_4@ZIF-8 carbon aerogel magnetic.

Table 2. Box-Behnken design matrix for variables and removal (%)values.

2.6. Nonlinear isotherms of adsorption and Thermodynamics Studies

The adsorption isotherms of Gasoil removal by cellulose@Fe_3O_4@ZIF-8 carbon aerogel magnetics were studied at various temperatures and initial Gasoil concentrations. The Langmuir, Freundlich, Temkin, and Azizian et al isotherms were used to correlate the data to find the best adsorption model. The nonlinear Langmuir isotherm is Eq. 3.

$$q_e = \frac{q_m K_L C_e}{1 + K_L C_e} \quad (3)$$

where K_L (L.g^{-1}) is the Langmuir constant, C_e is the equilibrium concentration, and q_m (g.g^{-1}) is the maximum adsorption capacity, once a compelete monolayer of adsorbent covers the surface (Langmuir 1918). The Freundlich isotherm is represented by Eq. 4, where K_F is the Freundlich constant. The constant 1/*n* (with a value between 0 and 1) is related to the surface heterogeneity, and the closer this value is to 1 the more homogeneous the surface is (Freundlich 1907).

$$q_e = K_F C_e^{\frac{1}{n}} \qquad (4)$$

Temkin studied surface adsorption isotherm interactions. The findings have shown that due to these interactions, the adsorption heat of all monolayer molecules diminishes linearly with the surface coverage. Such an effect comes from the repulsive forces on a homogeneous surface or from the inhomogeneity of the surface. This isotherm is represented by Eq. 5, where parameters A and B are Temkin equilibrium constants (Xia et al. 2021).

$$q_e = BlnA + BlnC_e \qquad (5)$$

However, Azizian et al isotherm suggests a revised Langmuir isotherm that better explains dense phase of desorption and adsorption processes. Adsorption thermodynamic parameters may be calculated on a global scale with the help of this method. C_S and K_{ML} parameters are concentration saturation and modified Langmuir coefficient (Azizian et al. 2018).

$$q_e = \frac{q_m K_{ML} C_e}{C_s + (K_{ML} - 1) C_e} \qquad (6)$$

The thermodynamics of Gasoil removal by cellulose@Fe_3O_4@ZIF-8 carbon aerogel magnetic was investigated at different temperatures. Calculation of enthalpy, entropy and Gibbs free energy changes (*ΔH*, *ΔS*, and *ΔG*) are necessary to understand adsorption spontaneity, practicability, and foundations. Using the Van't Hoff equation, we can get the values of these parameters (Azizian et al. 2018):

$$\Delta G = -RTlnK_{ML} \qquad (7)$$

$$lnK_{ML} = \frac{\Delta S}{R} - \frac{\Delta H}{RT} \quad (8)$$

The dimensionless K_{ML} is the modified Langmuir coefficient that may be derived using the Azizian et al isotherm.

3. Results and discussion

3.1. FT-IR Spectroscopy

Figure 1 presents the FTIR spectra of cellulose@Fe_3O_4@ZIF-8 carbon aerogel magnetic. The absorption spectra of the sample showed peaks at 1558, 1003.2, and 872.2 cm^{-1}, which correspond to C=O, N-O, C-N, Zn-O, and Fe-O, respectively. The band at 872.2 cm^{-1} represents the stretching vibration of the Fe-O bond, indicating FeO_x in the aerogel's carbonaceous phase. This band also shows the formation of the ZIF-8 structure. The 2923 cm^{-1} band represents cellulose's hydroxyl and carboxyl stretching vibrations. The functional groups identified in the sample can participate in the surface adsorption of Gasoil.

Figure 1. FT-IR spectrum of cellulose@Fe_3O_4@ZIF-8 carbon aerogel magnetic.

3.2. SEM and EDS analyses

SEM pictures of cellulose@Fe_3O_4@ZIF-8 magnetic carbon aerogel are shown in Figure 2. Examining the SEM images shows that the adsorbents structure has many pores and gaps suitable for adsorbing Gasoil and removing it from the aqueous solution. The formation of adsorbent nanoparticles provides more access to the adsorption sites. Figure 3 shows EDS analysis, which confirms the presence of Fe, O, and Zn elements in the adsorbent.

Figure 2. SEM images of (a) surface structures of PF-carbon and (b, c, d) cellulose@Fe_3O_4@ZIF-8 carbon aerogel magnetic.

Figure 3. The spectrum obtained from sample analysis by the X-ray energy dispersion (EDS) method.

3.3. X-ray Diffraction (XRD)

Figure 4 displays the pre- and post-adsorption XRD patterns of cellulose@Fe_3O_4@ZIF-8 carbon aerogel magnetic, MAA-Fe_3O_4, and PF cellulose carbon. Figure 4c shows the magnetic carbon aerogel's XRD patterns are identical to those of MAA-Fe_3O_4 (Figure 4a) and PF cellulose carbon (Figure 4b). Figure 4c shows the XRD pattern of cellulose@Fe_3O_4@ZIF-8 carbon aerogel magnetic, which reveals a strong peak at $2\theta=35^{o}$. The absence of change in the XRD patterns before (Figure 4c), and after (Figure 4d) adsorption demonstrates the adsorbent's high stability in Gasoil adsorption, and its structure is unaltered throughout the adsorption process.

Figure 4. XRD patterns of (a) MAA- Fe_3O_4, (b) Cellulose carbon of PF, (c) cellulose@Fe_3O_4@ZIF-8 carbon aerogel magnetic before adsorption and, (d) cellulose@Fe_3O_4@ZIF-8 carbon aerogel magnetic after adsorption.

3.4. Vibrating-Sample Magnetometer (VSM)

The magnetic hysteresis loop tests a magnetic aerogel's reaction to a magnetic field. It is shown as a curve of change of magnetization of the material concerning the applied area. The residual loop relies on magnetic field direction, sample ratio, sample extent, material type, and magnetic return method. Figure 5 demonstrates the hysteresis loop under the field -15000 to +15000 Oe. The cellulose@Fe_3O_4@ZIF-8 carbon aerogel magnetic hysteresis curves showed super magnetic adsorption. The meausred saturation magnetization (*Ms*) and magnetic remanence (*Mr*) were 5.83 and 0.7081 emu.g^{-1}, respectively. An external magnet can easily extract cellulose@Fe_3O_4@ZIF-8 carbon aerogel magnetic from the solution.

Figure 5. Hysteresis curve of cellulose@Fe_3O_4@ZIF-8 carbon aerogel magnetic

3.5. Inductively coupled plasma emission spectrometry (ICP)

During adsorption, ion leaching from the adsorbent was investigated using ICP. The findings show that the quantity of iron in the adsorbent decreases from 5.06 % before adsorption to 4.06% after adsorption. Also, the amount of zinc before adsorption is 3.88%, which reaches 1.2% after adsorption. This finding demonstrates the durability and presence of magnetic characteristics in the adsorbent following the adsorption process.

3.6. Optimizing adsorption parameters using Box-Benken design

The dependence between parameters A, B, C, and the response parameter (R%) was obtained as follows:

$$R(\%) = 44.41+(9.98\times A) - (31.34\times B) + (1.38C) - (1.8\times AB) - (0.1450\times A\times C) - (0.1175\times B\times C) + (0.1888\times A\times A) + (13.73\times B\times B) + (0.9612\times C\times C) \quad (9)$$

According to Eq. 9, the weight of the adsorbent has a favorable effect on adsorption efficiency. This equation shows the adsorbent weight's significant impact on the adsorption reaction. The experimental and predicted Gasoil removal values are similar (%R= 98.99 and 94.2, respectively), and showing the model's power.

Pareto diagrams may also determine each factor's relevance by estimating its percentage influence on the solution (Khataee et al. 2011). The Pareto chart analysis for removing Gasoil by cellulose@Fe_3O_4@ZIF-8 carbon aerogel magnetic adsorbent is shown in Figure 6. As seen in Figure 6, the factors B (76.9476), B×B (14.7686), A (7.8029), and C×C (5.3743) are the most influential parameters on the adsorption of Gasoil by cellulose@Fe_3O_4@ZIF-8 carbon aerogel magnetic.

Figure 6. Pareto graphic analysis.

When a function has two constant parameters, response surfaces are given. The significant and interaction impacts of these two parameters may be better understood. The effect of these factors on Gasoil extraction is seen in Figure 7. Magnetic carbon aerogel adsorbs the most Gasoil at 0.1 g of adsorbent (A) and 0.5 g of Gasoil. The cellulose@Fe_3O_4@ZIF-8 carbon aerogel magnetic has successfully adsorbed 100% Gasoil under these circumstances. The projected and Gasoil removal values are shown in Figure 8. The clustering of the dots along a line provides more evidence of the robust pattern.

Figure 7. Response surface plot for the effects of the adsorbent weight (A) and initial Gasoil weight (B).

Figure 8. Actual vs. predicted values of the Gasoil removal.

3.7. Adsorption isotherms and thermodynamics studies

At 30, 40, and 50°C, the nonlinear isotherms of Gasoil adsorption by cellulose@Fe_3O_4@ZIF-8 carbon aerogel magnetic were investigated. The results of the nonlinear fitting of Langmuir, Freundlich, Temkin, and Azizian et al isotherms using the solver plugin in the Excel program are presented in Table 3. The saturated concentration (C_s) of Gasoli in water was considered to be 0.35 g.L^{-1} (Winkler 2009). The obtained corresponding correlation coefficients (R^2) showed the process of Gasoil adsorption. The magnetic carbon aerogel exhibits nonlinear Freundlich isotherm-like adsorption. Figure 9 shows the adsorption capacity regarding equilibrium concentration at different temperatures. As the temperature rises, so does the ability for adsorption, whereas, at lower temperatures, adsorption is enhanced.

Table 3. Nonlinear fitting parameters of adsorption isotherm models.

Figure 9. Isotherm curve of Gasoil adsorption on cellulose@Fe_3O_4@ZIF-8 carbon aerogel magnetic.

Figure 10 depicts a fitting curve for lnK_{ML} *vs.* 1/T. The thermodynamic parameters are shown in Table 4. Since the value of ΔH is negative, adsorption is an exothermic reaction.

When ΔS is positive, it indicates that the degree of disorder has grown. Negative ΔG at a given temperature suggests the adsorption occurs spontaneously and it has a thermodynamic benefit. This result is in line with the theory that decreasing the temperature enhances adsorption.

Table 4. Thermodynamic parameters of Gasoil adsorption using cellulose@Fe_3O_4@ZIF-8 carbon aerogel magnetic.

Figure 10. The fitting curve of $\ln K_{ML}$ versus *1/T*.

3.8. Adsorption mechanism

The adsorption mechanism involves the various physical and chemical interactions between the adsorbate and the adsorbent. The interactions or forces can be electrostatic, hydrogen, vander Waals, coordination, or covalent. Unraveling the adsorption mechanism is crucial for optimizing the adsorption performance and designing more efficient adsorbents. The cellulose@Fe_3O_4@ZIF-8 carbon aerogel magnetic exhibits excellent adsorption efficiency for Gasoil removal from water, which can be attributed to several factors. These include electrostatic interactions between the negatively charged surface of the composite material and the positively charged Gasoil molecules, hydrogen bonding between the organic linkers of the MOF and gasoil molecules, and the porous nature of the composite material, which facilitates the rapid diffusion of Gasoil.

The synthesized adsorbent is very hydrophobic and has a high affinity for adsorbing Gasoil. The Gasoil is adsorbed into the sponge-and-Aerogel -structure sorbent in a short amount of time and then separated from the water. The data show that Gasoil spontaneously and physically adsorbed onto synthetic aerogel adsorbents. To perform physisorption, Gasoil must fill the pores of the aerogel. Since low-density aerogel constantly floats on the water's surface, the whole adsorption process occurs at the bottom.

3.9. Regeneration and reusability

The regeneration and reusability of the cellulose@Fe_3O_4@ZIF-8 carbon aerogel magnetic composite is essential for long-term and practical applications. The composite can be regenerated using a suitable desorption agent, such as NaOH, which allows for the recovery and reuse of the adsorbent material. The regeneration process can be performed multiple times, ensuring the long-term performance and cost-effectiveness of the composite for Gasoil removal.

The adsorption performance of the aerogel was estimated after eight consecutive cycles of utilization (Figure 11). The findings show that after eight uses, the adsorbent has a strong adsorption capacity. After eight cycles, the recycled adsorbent's capacity was evaluated. After eight times of uses, the adsorbent had a high adsorption capacity, and only around 10 % of its adsorption capacity was degraded. This property of magnetic carbon aerogel is precious.

Figure 11. Regeneration and reusability of cellulose@Fe_3O_4@ZIF-8 carbon aerogel magnetic.

3.10. Comparison with other adsorbents

Various adsorbents can remove Gasoil from aqueous solutions. Table 5 shows some examples of these adsorbents with their adsorption capacities. Overall, while there is limited research specifically comparing the effectiveness of cellulose@Fe_3O_4@ZIF-8 carbon aerogel magnetic to other adsorbents in removing Gasoil from water, the studies suggest that ZIF-8 and cellulose-based composites can be effective adsorbents for removing Gasoil from water.

Table 5. Comparison of the maximum adsorption capacities of Gasoil by different adsorbents.

4. Conclusion

In summary, the Biomass@Fe_3O_4@ZIF-8 adsorbent was synthesized through the in-situ growth of ZIF-8 on Fe_3O_4-modified cellulosic fibers, exhibits excellent Gasoil removal efficiency from aqueous solutions. The adsorption process was optimized using the Box-Behnken method, and the adsorption isotherms and thermodynamics were studied to understand the underlying mechanism. The adsorbent demonstrated a good reusability and environmental compatibility, making it a promising candidate for Gasoil removal in real-world applications.

The resulting adsorbent is a superhydrophobic polymer that efficiently removes water from Gasoil. Under an external magnetic field, the saturated adsorbent is rapidly separated from the water without filtration or centrifugation. This adsorbent helps to save time, money, and materials. Only approximately 10% of the sorbent's adsorption ability is lost after eight reuses, so it still has plenty of life.

The removal efficiency of Gasoil was studied using DOE to determine the optimal sorbent weight, starting Gasoil weight, and solution pH. By studying the impacts of numerous parameters on Gasoil removal, the starting concentration and adsorbent weight had the most significant influence. Using 0.5 g of Gasoil weight and 0.1 g of adsorbent weight is ideal for Gasoil removal. Under ideal circumstances, magnetic aerogels composed of cellulose@Fe_3O_4@ZIF-8 can remove all traces of Gasoil from the water. After entering the sponge and aerogel sorbent, Gasoil is quickly separated from water. The Gasoil removal capability of the adsorbent is very high (7 $g.g^{-1}$) in aqueous solutions.

References

Abdelhamid HN, Mathew AP (2022): Cellulose–metal organic frameworks (CelloMOFs) hybrid materials and their multifaceted Applications: A review. Coordination Chemistry Reviews 451: 214263

Abdelmigeed MO, Sadek AH, Ahmed TS (2022): Novel easily separable core-shell Fe_3O_4/PVP/ZIF-8 nanostructure adsorbent: optimization of phosphorus removal from Fosfomycin pharmaceutical wastewater. RSC Adv 12: 12823-12842

Ali MA, Shaaban-Dessuuki SA, El-Wassefy NA, Mostafa SI, Hussein MH (2021): Adsorption of crude and waste diesel oil onto agar-carboxymethylcellulose-silver nanocomposite in aqueous media. Inorg. Chem. Commun. 133: 108915

Arabameri M, Bashiri H (2022): Introduction of the Effective Photon Concentration Variable for Studying the Mechanism of Crystal Violet Photodegradation. Photochem. Photobiol. 98: 798-814

Azizian S, Eris S, Wilson LD (2018): Re-evaluation of the century-old Langmuir isotherm for modeling adsorption phenomena in solution. Chem. Phys. 513: 99-104

Bashiri H, Nesari S, Sarabadan M (2020): Microwave assistant production of a high performance adsorbent from rice husk. Korean J. Chem. Eng. 37: 240-248

Bui T, Nguyen C, Hua S, Chun H, Kim YS (2022a): Sonochemical Preparation of a Magnet-Responsive Fe_3O_4@ZIF-8 Adsorbent for Efficient Cu^{2+} Removal. Nanomaterials 12: 753

Bui TT, Nguyen DC, Hua SH, Chun H, Kim YS (2022b): Sonochemical Preparation of a Magnet-Responsive Fe_3O_4@ZIF-8 Adsorbent for Efficient Cu^{2+} Removal. Nanomaterials (Basel) 12

Cai L, Zhang Y, Zhou Y, Zhang X, Ji L, Song W, Zhang H, Liu J (2019): Effective adsorption of diesel oil by crab-shell-derived biochar nanomaterials. Materials 12: 236

Chen LF, Wang HH, Lin KY, Kuo JY, Wang MK, Liu CC (2018): Removal of methylene blue from aqueous solution using sediment obtained from a canal in an industrial park. Water Sci Technol 78: 556-570

Ewis D, Benamor A, Ba-Abbad MM, Nasser M, El-Naas M, Qiblawey H (2020): Removal of oil content from oil-water emulsions using iron oxide/bentonite nano adsorbents. Journal of Water Process Engineering 38: 101583

Ewis D, Mahmud N, Benamor A, Ba-Abbad MM, Nasser M, El-Naas M (2022): Enhanced Removal of Diesel Oil Using New Magnetic Bentonite-Based Adsorbents Combined with Different Carbon Sources. Water, Air, Soil Pollut. 233: 195

Falaki Z, Bashiri H (2021): Preparing an adsorbent from the unused solid waste of Rosewater extraction for high efficient removal of Crystal Violet. Journal of the Iranian Chemical Society 18: 2689-2702

Freundlich H (1907): Über die adsorption in lösungen. Zeitschrift für physikalische Chemie 57: 385-470

Gorkunov M, Lapine M, Shamonina E, Ringhofer K (2002): Effective magnetic properties of a composite material with circular conductive elements. The European Physical Journal B-Condensed Matter and Complex Systems 28: 263-269

Han X, Wu Z, Yang Y, Guo J, Wang Y, Cai L, Song W, Ji L (2021): Facile Preparation of a Porous Biochar Derived from Waste Crab Shell with High Removal Performance for Diesel. Journal of Renewable Materials 9: 1377-1391

Jabbar SQ, Janani H, Janani H (2022): Cellulose-Based Hybrid Composites Enabled by Metal Organic Frameworks for CO_2 Capture: The Effect of Cellulosic Substrate. Journal of Polymers and the Environment 30: 4210-4224

Jafarinejad A, Salavati-Niasari M, Monsef R, Bashiri H (2023): Flower-shaped magnetically recyclable ZnS/ZnIn2S4/Fe2O3 nanocomposites towards decolorization of colored pollutants. Int. J. Hydrogen Energy 48: 3440-3455

Karimi M, Mehrabadi Z, Farsadrooh M, Bafkary R, Derikvandi H, Hayati P, Mohammadi K (2021): Chapter 4 - Metal–organic framework. In: Ghaedi M (Editor), Interface Science and Technology. Elsevier, pp. 279-387

khalilifard M, Javadian S (2021): Magnetic superhydrophobic polyurethane sponge loaded with Fe_3O_4@oleic acid@graphene oxide as high performance adsorbent oil from water. Chemical Engineering Journal 408: 127369

Khataee A, Zarei M, Khataee A (2011): Electrochemical Treatment of Dye Solution by Oxalate Catalyzed Photoelectro-Fenton Process Using a Carbon Nanotube-PTFE Cathode: Optimization by Central Composite Design. CLEAN – Soil, Air, Water 39: 482-490

Kuwer P, Yadav A, Labhasetwar PK (2021): Adsorption of cupric, cadmium and cobalt ions from the aqueous stream using the composite of iron(II,III) oxide and zeolitic imidazole framework-8. Water Science and Technology 84: 2288-2303

Langmuir I (1918): The adsorption of gases on plane surfaces of glass, mica and platinum. Journal of the American Chemical society 40: 1361-1403

Li N, Zhou L, Jin X, Owens G, Chen Z (2019): Simultaneous removal of tetracycline and oxytetracycline antibiotics from wastewater using a ZIF-8 metal organic-framework. Journal of Hazardous Materials 366: 563-572

Liu J, Li Y, Lou Z (2022): Recent Advancements in MOF/Biomass and Bio-MOF Multifunctional Materials: A Review. Sustainability 14: 5768

Liu X, Xiao Y, Zhang Z, You Z, Li J, Ma D, Li B (2021): Recent Progress in Metal-Organic Frameworks@ Cellulose Hybrids and Their Applications. Chinese Journal of Chemistry 39: 3462-3480

Moghaddam M, Nabizadeh R, Dehghani MH, Akbarpour B, Azari A, Yousefi M (2019): Performance investigation of Zeolitic Imidazolate Framework – 8 (ZIF-8) in the removal of trichloroethylene from aqueous solutions. Microchemical Journal 150: 104185

Nadar SS, Rathod VK (2018): Magnetic-metal organic framework (magnetic-MOF): A novel platform for enzyme immobilization and nanozyme applications. Int J Biol Macromol 120: 2293-2302

Oliveira LC, Rios RV, Fabris JD, Garg V, Sapag K, Lago RM (2002): Activated carbon/iron oxide magnetic composites for the adsorption of contaminants in water. Carbon 40: 2177-2183

Paz R, Viltres H, Gupta NK, Leyva C, Dhavale RP, Park H-H, Romero-Galarza A, Rajabzadeh AR, Srinivasan S (2023): Fabrication of metal-organic frameworks with trimesic linkers for europium adsorption and recovery from aqueous solutions. Journal of Environmental Chemical Engineering 11: 110084

Sarabadan M, Bashiri H, Mousavi SM (2019): Removal of crystal violet dye by an efficient and low cost adsorbent: Modeling, kinetic, equilibrium and thermodynamic studies. Korean J. Chem. Eng. 36: 1575-1586

Shi M, Huang R, Qi W, Su R, He Z (2020): Synthesis of superhydrophobic and high stable Zr-MOFs for oil-water separation. Colloids and Surfaces A: Physicochemical and Engineering Aspects 602: 125102

Simon YDT, Hadis B, Estella TN, Arabamiri M, Serges D, Arnaud KT, Samuel L, Minoo T, Michael S, Reinhard S (2020): Urea and green tea like precursors for the preparation of g-C_3N_4 based carbon nanomaterials (CNMs) composites as photocatalysts for photodegradation of pollutants under UV light irradiation. Journal of Photochemistry and Photobiology A: Chemistry: 112596

Sun S, Jiang Q, Zhang W, Tian L, Li T, Zheng L, Gao Y, Zeng X, Zhou L (2022): Efficient adsorption of tetracycline in aquatic system by thermally-treated sediment. Environ. Res. 214: 113779

Tajari E, Bashiri H (2023): Gasoil removal from aqueous solution using magnetic metal-organic framework adsorbent based on the cellulosic fibrous of Prosopis farcta plant. Int J Biol Macromol 245: 125473

Tao Y, Du J, Cheng Y, Lu J, Min D, Wang H (2023): Advances in Application of Cellulose-MOF Composites in Aquatic Environmental Treatment: Remediation and Regeneration. Int J Mol Sci 24

Tu K, Ding Y, Keplinger T (2022): Review on design strategies and applications of metal-organic framework-cellulose composites. Carbohydr Polym 291: 119539

Winkler I (2009): Investigation of the Oil-Products Solubility in Water: Qualitative Composition and Quantitative Limits of the Oil-Water Mixtures. In: Bahadir AM , Duca G (Hrsg.), The Role of Ecological Chemistry in Pollution Research and Sustainable Development. Springer Netherlands, Dordrecht, pp. 103-108

Wu Y, Li B, Wang X, Yu S, Pang H, Liu Y, Liu X, Wang X (2019): Magnetic metal-organic frameworks (Fe_3O_4@ZIF-8) composites for U(VI) and Eu(III) elimination: simultaneously achieve favorable stability and functionality. Chemical Engineering Journal 378: 122105

Xia J, Gao Y, Yu G (2021): Tetracycline removal from aqueous solution using zirconium-based metal-organic frameworks (Zr-MOFs) with different pore size and topology: Adsorption isotherm, kinetic and mechanism studies. Journal of Colloid and Interface Science 590: 495-505

Yadav S, Dixit R, Sharma S, Dutta S, Solanki K, Sharma RK (2021): Magnetic metal–organic framework composites: structurally advanced catalytic materials for organic transformations. Materials Advances 2: 2153-2187

Yu Z, Ding K, Han C, Wu Y, Zou M, Liu Y, Guan F (2021): Adsorption of diesel oil onto natural mud shale: from experimental investigation to thermodynamic and kinetic modelling. Int. J. Environ. Anal. Chem.: 1-15

Zeng X, Zhang G, Zhu J (2022): Selective adsorption of heavy metals from water by a hyper-branched magnetic composite material: Characterization, performance, and mechanism. Journal of Environmental Management 314: 114979

Zhao X, Liu S, Tang Z, Niu H, Cai Y, Meng W, Wu F (2015a): Synthesis of magnetic metal-organic framework (MOF) for efficient removal of organic dyes from water. Scientific reports 5: 11849

Zhao X, Liu S, Tang Z, Niu H, Cai Y, Meng W, Wu F, Giesy JP (2015b): Synthesis of magnetic metal-organic framework (MOF) for efficient removal of organic dyes from water. Scientific reports 5: 11849

Zheng J, Cheng C, Fang W-J, Chen C, Yan R-W, Huai H-X, Wang C-C (2014): Surfactant-free synthesis of a Fe_3O_4@ZIF-8 core–shell heterostructure for adsorption of methylene blue. Christendom 16: 3960-3964

Zhou S, Kong X, Zheng B, Huo F, Strømme M, Xu C (2019): Cellulose Nanofiber @ Conductive Metal–Organic Frameworks for High-Performance Flexible Supercapacitors. ACS Nano 13: 9578-9586

Ethics approval and consent to participate

Not applicable.

Consent for publication

Not applicable.

Authors contributions

Conception and design of study: H. Bashiri

Collected the data, analysis and/or interpretation of data: E. Tajari

Wrote the manuscript: E. Tajari

All authors read and approved the final manuscript.

Funding

Our thanks to the University of Kashan for Grant No. (1143438/4).

Competing Interest

We wish to draw the attention of the Editor to the following facts, which may be considered as potential conflicts of interest and to significant financial contributions to this work. We confirm that the manuscript has been read and approved by all named authors and that there are no other persons who satisfied the criteria for authorship but are not listed. We further confirm that all of us have approved the order of authors listed in the manuscript. We understand that the Corresponding Author is the sole contact for the Editorial process (including Editorial Manager and direct communications with the office). She is responsible for communicating with the other authors about progress, submissions of revisions and final approval of proofs. We confirm that we have provided a current, correct email address which is accessible by the Corresponding Author and which has been configured to accept email from (hbashiri@kashanu.ac.ir).

Tables:

Table 1.

Factors	**Name**	**Low**	**Middle**	**High**
		-1	0	+1
A	Adsorbent weight (g)	0.05	0.075	0.1
B	Gasoil weight (g)	0.5	0.75	2
C	pH	5	7.5	10

Table 2.

Run	**Coded value(A)**	**Coded value(B)**	**Coded value(C)**	**Removal (%)**
1	0.075	1.25	7.5	45.84
2	0.1	2	7.5	34.93
3	0.075	1.25	7.5	43.24
4	0.075	2	10	27.62
5	0.075	0.5	10	93.04
6	0.075	2	5	25.4
7	0.05	2	7.5	21.55
8	0.05	1.25	10	35.76
9	0.05	1.25	5	32.41
10	0.1	0.5	7.5	98.7
11	0.075	0.5	5	90.35
12	0.05	0.5	7.5	78.14
13	0.075	1.25	7.5	44.15
14	0.1	1.25	10	58.42
15	0.1	1.25	5	55.65

Table 3.

Models Isotherm	**parameter**	**value**
Langmuir	q_{max} (g.g^{-1})	6.99

	K_L (L.g^{-1})	2.68
	R^2	0.818
Freundlich	K_F (g.g^{-1}(g.L^{-1})$^{-\frac{1}{n}}$)	3.716
	n	6.377
	R^2	0.9399
Temkin	A (L.g^{-1})	24951.76
	B (g.g^{-1})	0.446
	R^2	0.9333
Azizian et al	K_{ML}	1.941
	q_m	3.041
	R^2	0.8180

Table 4.

T(K)	**ΔH**(J.mol^{-1})	**ΔS**(J.mol^{-1}.k^{-1})	**ΔG**(KJ.mol^{-1})
303.15			-5.917
313.15	-259.98	18.66	-6.103
323.15			-6.290

Table 5.

Adsorbent	Maximumadsorption capacity ($g.g^{-1}$)	References
Agar-CMC-Silver	0.895	(Ali et al. 2021)
Crab shell biochar (CSB)	0.0934	(Cai et al. 2019)
Natural mud shale	0.025	(Yu et al. 2021)
Crab shell biochar (CSB)	0.451	(Han et al. 2021)
Fe_3O_4/Bent/rGO	0.085	(Ewis et al. 2022)
Fe_3O_4/Bent/MWCNTs	0.077	(Ewis et al. 2022)
Fe_3O_4/Bentonite	0.054	(Ewis et al. 2020)
MIL-53(Fe)	4.3	(Tajari &Bashiri 2023)
Cellulose fibers of PF plant	1	(Tajari &Bashiri 2023)
cellulose@Fe_3O_4@ZIF-8 carbon aerogel magnetic	7	This work

Figures:

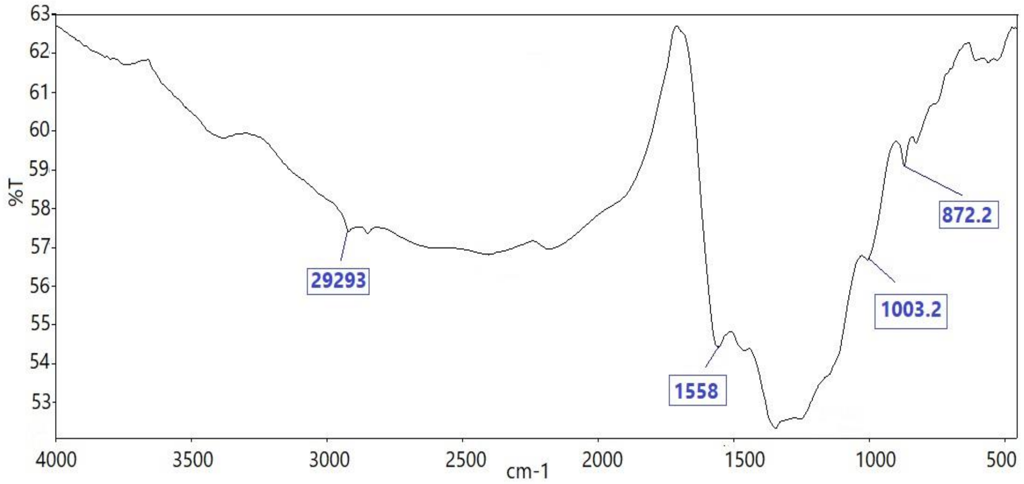

Figure 1.

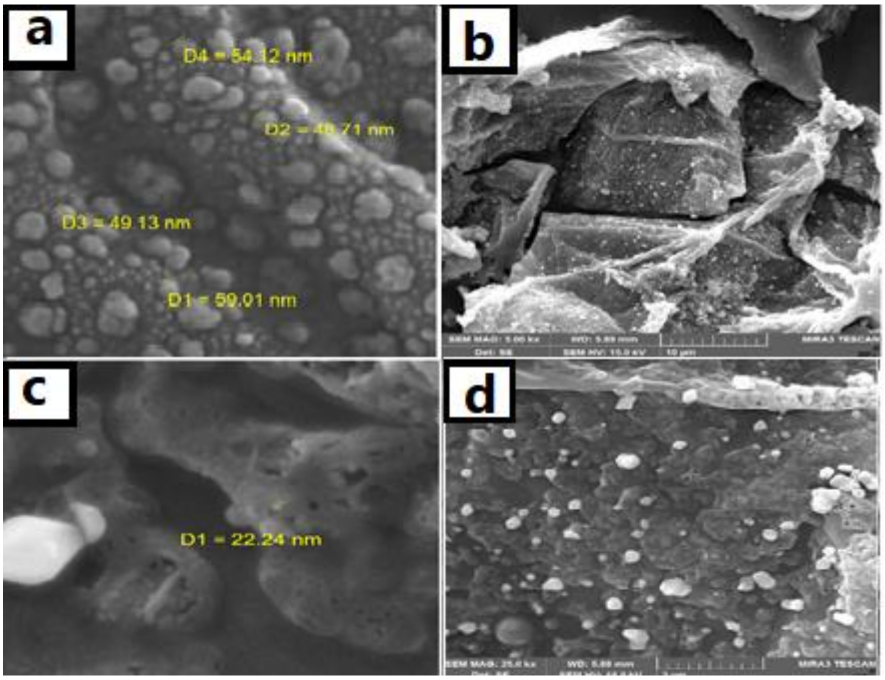

Figure 2.

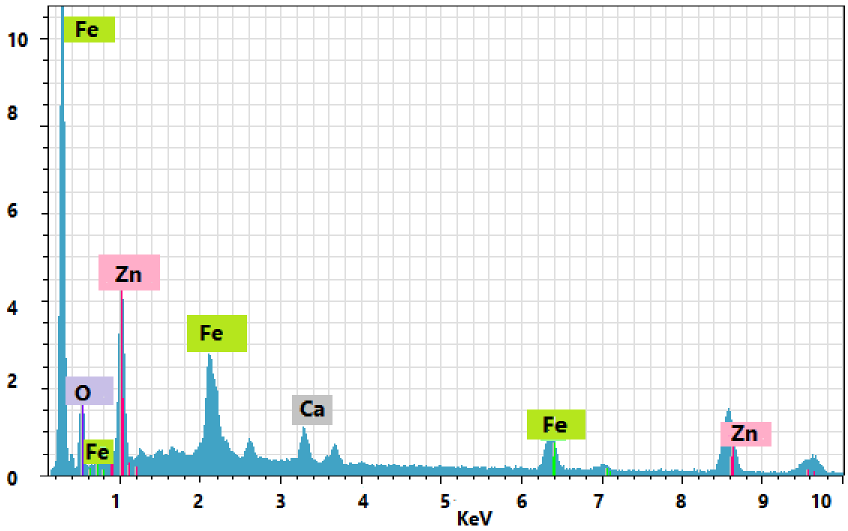

Figure 3.

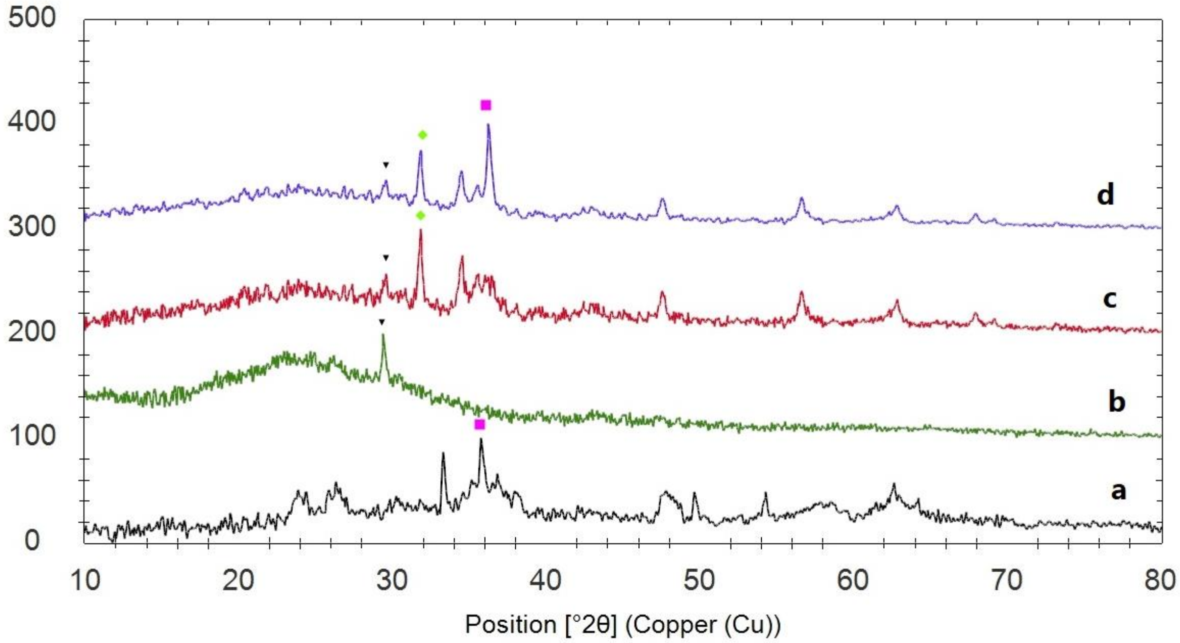
500
400
300
200
100
0
10
20
30
40
50
60
70
80
Position [°2θ] (Copper (Cu))
d
c
b
a

Figure 4.

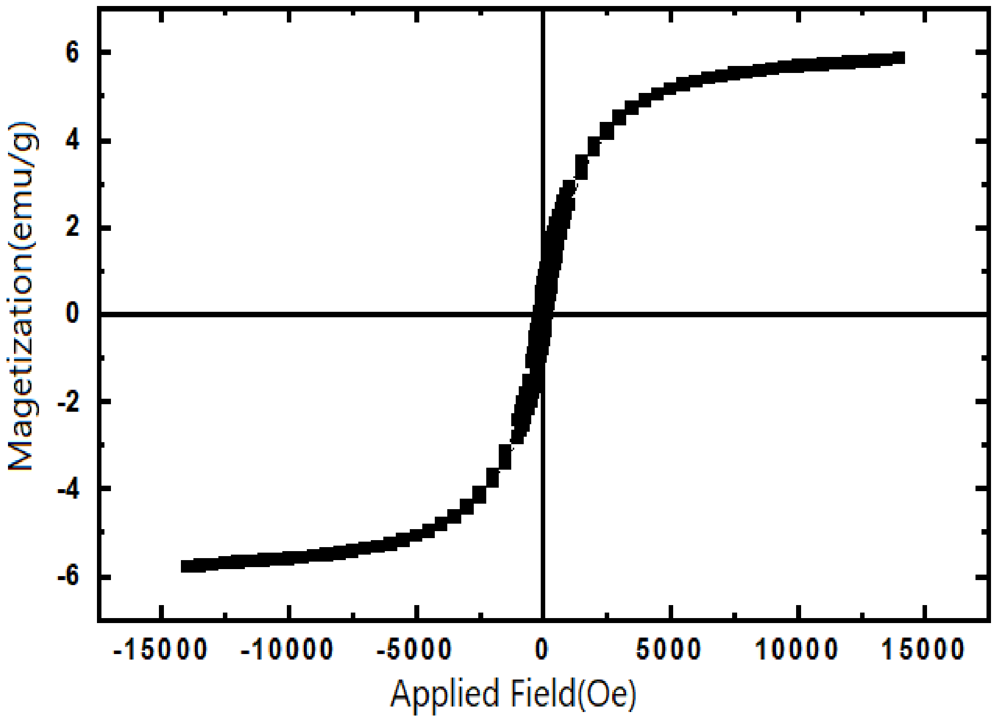
Magetization(emu/g)
Applied Field(Oe)
6
4
2
0
-2
-4
-6
-15000
-10000
-5000
0
5000
10000
15000

Figure 5.

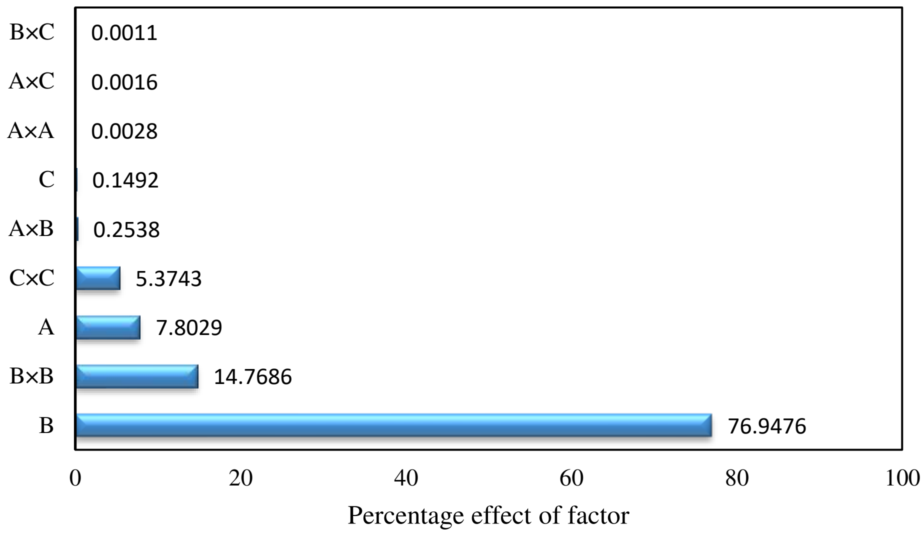
B×C
0.0011
A×C
0.0016
A×A
0.0028
C
0.1492
A×B
0.2538
C×C
5.3743
A
7.8029
B×B
14.7686
B
76.9476
0
20
40
60
80
100
Percentage effect of factor

Figure 6.

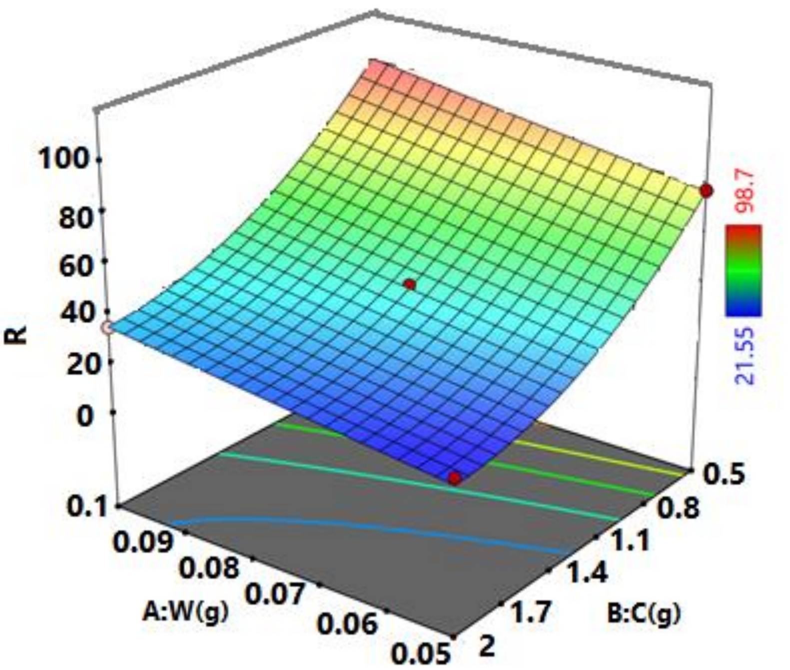
100
80
60
40
20
0
R
98.7
21.55
0.1
0.09
0.08
0.07
0.06
0.05
A:W(g)
0.5
0.8
1.1
1.4
1.7
2
B:C(g)

Figure 7.

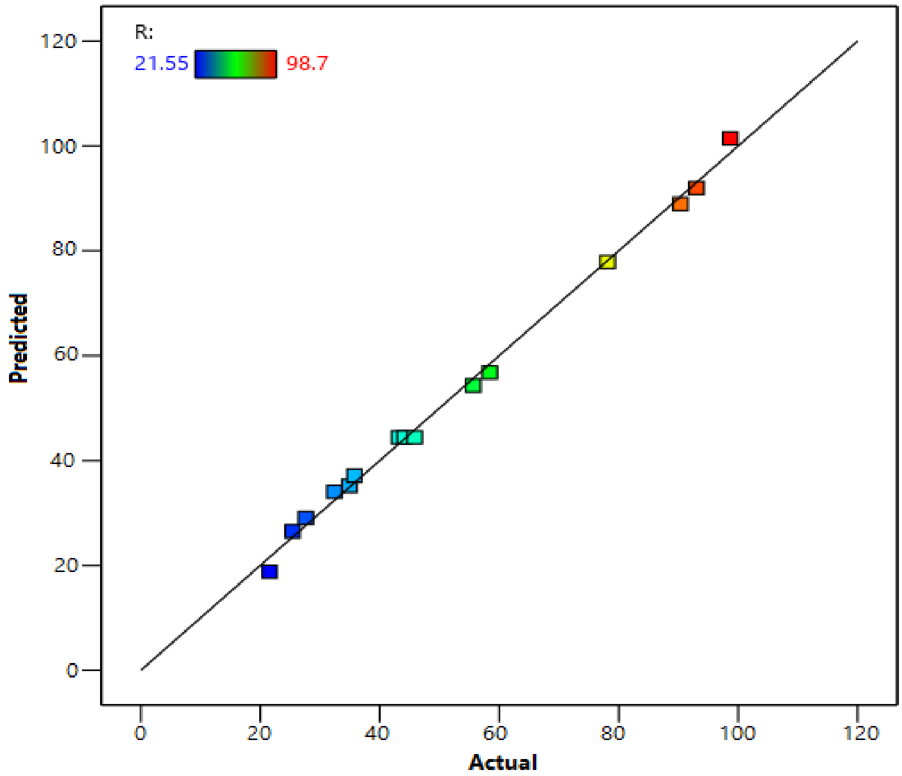
R:
21.55
98.7
120
100
80
60
40
20
0
Predicted
0
20
40
60
80
100
120
Actual

Figure 8.

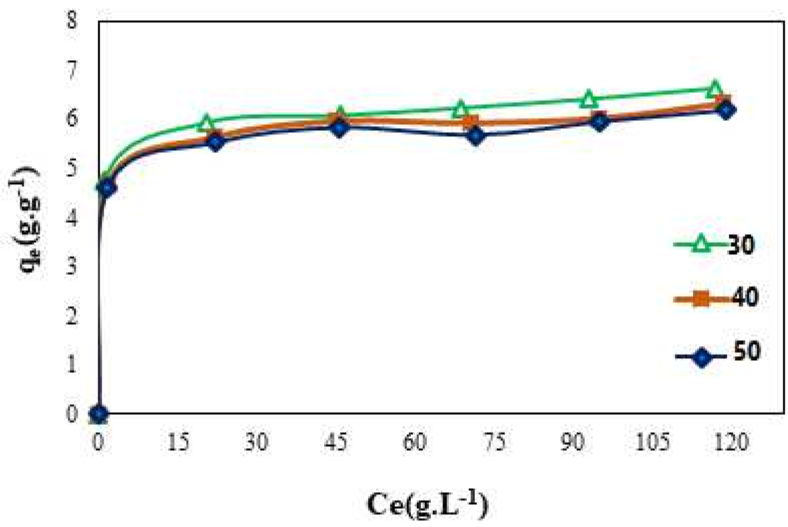

Figure 9.

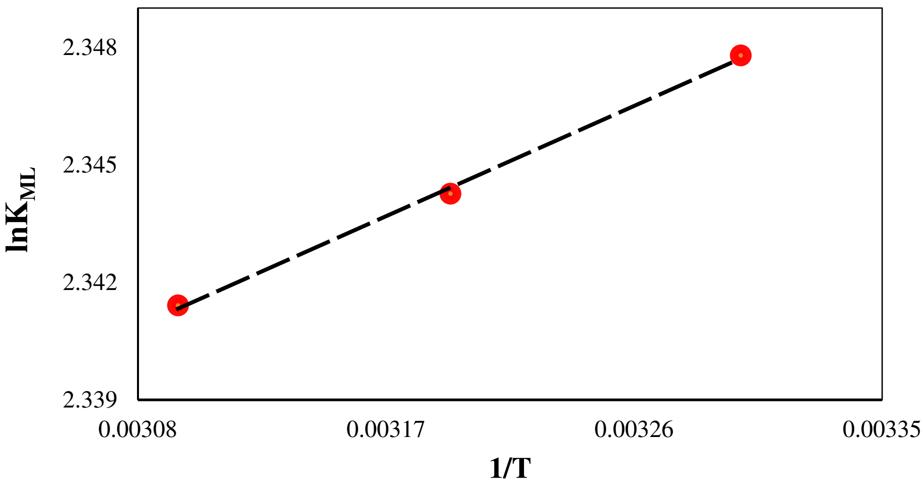

Figure 10.

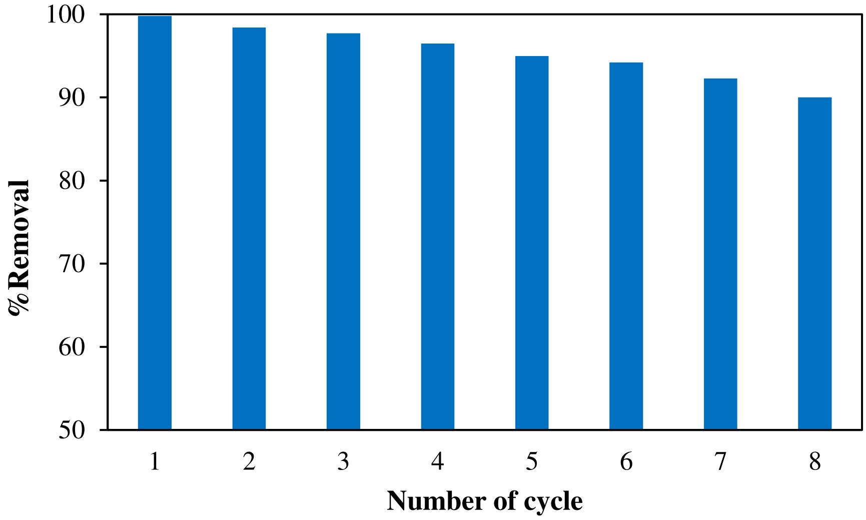

Figure 11.